Contents lists available at ScienceDirect

Experimental Cell Research

Research article

Neoplastic extracellular matrix environment promotes cancer invasion *in vitro*

Elias Sundquist [a,b,*], Outi Renko [c,1], Sirpa Salo [a,b,d], Johanna Magga [c], Nilva K. Cervigne [e], Pia Nyberg [a,b,f], Juha Risteli [a,g,h], Raija Sormunen [i,j], Olli Vuolteenaho [k], Flávia Zandonadi [l], Adriana F. Paes Leme [l], Ricardo D. Coletta [e], Heikki Ruskoaho [c,m], Tuula Salo [a,b,n]

[a] Cancer and Translational Medicine Research Unit, University of Oulu, PO Box 5281, Aapistie 5A, FIN 90014 Oulu, Finland
[b] Medical Research Center, Oulu University Hospital, Oulu, Finland
[c] Department of Pharmacology and Toxicology, Research Unit of Biomedicine, University of Oulu, Oulu, Finland
[d] Faculty of Biochemistry and Molecular Medicine, University of Oulu, Oulu, Finland
[e] Department of Oral Diagnosis, Oral Pathology Division, Piracicaba Dental School, University of Campinas, Campinas, Brazil
[f] Biobank Borealis of Northern Finland, Oulu University Hospital, Oulu, Finland
[g] Department of Clinical Chemistry, Institute of Diagnostics, University of Oulu, Oulu, Finland
[h] Northern Laboratory Centre NordLab, Oulu University Hospital, Oulu, Finland
[i] Biocenter Oulu, Oulu, Finland
[j] Department of Pathology, Institute of Diagnostics, University of Oulu, Oulu, Finland
[k] Department of Physiology, Institute of Biomedicine, University of Oulu, Oulu, Finland
[l] Mass Spectrometry Laboratory, Brazilian Biosciences National Laboratory-CNPEM, Campinas, Brazil
[m] Division of Pharmacology and Pharmacotherapy, University of Helsinki, Helsinki, Finland
[n] Department of Oral and Maxillofacial Diseases, University of Helsinki, and HUSLAB, Helsinki, Finland

ARTICLE INFO

ABSTRACT

The invasion of carcinoma cells is a crucial feature in carcinogenesis. The penetration efficiency not only depends on the cancer cells, but also on the composition of the tumor microenvironment. Our group has developed a 3D invasion assay based on human uterine leiomyoma tissue. Here we tested whether human, porcine, mouse or rat hearts as well as porcine tongue tissues could be similarly used to study carcinoma cell invasion *in vitro*. Three invasive human oral tongue squamous cell carcinoma (HSC-3, SCC-25 and SCC-15), melanoma (G-361) and ductal breast adenocarcinoma (MDA-MB-231) cell lines, and co-cultures of HSC-3 and carcinoma-associated or normal oral fibroblasts were assayed. Myoma tissue, both native and lyophilized, promoted invasion and growth of the cancer cells. However, the healthy heart or tongue matrices were unable to induce the invasion of any type of cancer cells tested. Moreover, when studied in more detail, small molecular weight fragments derived from heart tissue rinsing media inhibited HSC-3 horizontal migration. Proteome analysis of myoma rinsing media, on the other hand, revealed migration enhancing factors. These results highlight the important role of matrix composition for cancer invasion studies *in vitro* and further demonstrate the unique properties of human myoma organotypic model.

© 2016 Elsevier Inc. All rights reserved.

1. Introduction

Cancer cell invasion is the first fatal step towards metastases which mostly leads to the patients' death. Therefore, the invasion activity of the tumor cells serves as an important prognostic factor in cancers [13,14]. Currently *in vitro* and *in vivo* studies concentrate the attention mainly on characterization of the genetic profile and proliferative activities of cancer cells. However, while mutation landscape and the cell proliferation rate are important in carcinogenesis, they alone are not sufficient factors to define the

severity of the disease. Indeed, in many cancers the pattern of extracellular matrix (ECM) invasion is a more significant prognosticator than the mitotic activity of the cells [4]. In the fibroblastic invasion pattern, elongated mesenchymal cells have increased traction forces that reorganize and degrade the ECM [27,32]. In addition to the proteolytic remodeling of ECM, some cancers adopt amoeboid migration characteristics and invade mainly using biomechanical forces. Eventually the crosstalk between the ECM and the cancer cells determine the invasion efficiency. Therefore, the tumor microenvironment (TME) containing e.g. cancer-associated fibroblasts (CAFs), endothelial and inflammatory cells; cytokines and proteases, is getting in the focus of cancer research [3,14].

In vitro, the 3D invasion pattern has been studied with organotypic models composed of rat tail type I collagen as well as commercial mouse tumor derivatives, such as Matrigel [21]. However, these classical methods that combine matrix from different species do not accurately mimic the composition of human TME. Our group has developed a 3D invasion assay using human uterine leiomyoma tissue [23]. This model, applied already in more than 20 publications, provides a hypoxic matrix containing essential TME components for in vitro invasion experiments [1,2,5,8,15,24,30,31,33]. In myoma tissue, invasion efficiency can be analyzed by determining the collagen degradation (carboxyterminal peptide of type I or III collagen - ICTP or IIICTP - radioimmunoassay measurements from the culture media) together with histological and immunohistological staining of the tissue sections [23]. The latter method elucidates the cancer cell growth pattern and the former determines whether proteolytic ECM degradation or amoeboid movement predominates in the invasion process.

In this study, we compared the suitability of heart or tongue solid tissue discs to myoma discs for cancer invasion assays. We also elucidated whether lyophilized and rehydrated myoma retains its invasion inductive properties. Finally, we tested the effects of the rinsing media (RM) from myoma and heart tissue discs on the migration of tongue carcinoma cells.

2. Materials and methods

2.1. Cell culture

Three different oral tongue squamous cell carcinoma (OTSCC) cell lines were used in this study: SCC-15 (ATCC® CRL-1623™, LGC Standards AB, Boras, Sweden), SCC-25 (ATCC® CRL-1628™, LGC Standards AB) and HSC-3 (JCRB 0623, Osaka National Institute of Health Sciences, Osaka, Japan). The cells were cultivated in DMEM/ F-12 (Invitrogen, Carlsbad, CA) with 10% heat-inactivated fetal bovine serum (FBS) (Perbio Science, Erembodegem, Belgium), 100 U/ml penicillin, 100 µg/ml streptomycin, 50 µg/ml ascorbic acid, 250 ng/ml Fungizone, 5 µg/ml insulin (bovine pancreas) and 0.4 ng/ml hydrocortisone (supplements from Sigma-Aldrich, Ayrshire, UK). The cells were cultivated in a humidified atmosphere of 5% CO_2 at 37 °C and passaged routinely using trypsin-EDTA (Sigma-Aldrich). Carcinoma-associated fibroblasts (CAFs), CaDEC12, were a kind gift from Dr. Daniela Costea, University of Bergen, Norway. CAFs were derived from a specimen of OTSCC [11]. CaDEC12 were cultivated in high-glucose DMEM (Sigma-Aldrich) with 100 U/ml penicillin, 100 µg/ml streptomycin, 50 µg/ml ascorbic acid, 250 ng/ml Fungizone, 1 mmol/L sodium pyruvate, and 10% heat-inactivated FBS. Normal oral fibroblasts (NOF) were isolated from normal superfluous buccal mucosa tissue after wisdom tooth extraction [10]. NOFs were cultivated similarly to CAFs. Malignant melanoma cells G-361 (ATCC® CRL-1424™, LGC Standards AB) and breast adenocarcinoma cells MDA-MB-231 (ATCC®

HTB-26™, LGC Standards AB) from metastatic sites were also used. G-361 cells were cultivated in CAF media and MDA-MB-231 cells in HSC-3 media, both described above.

2.2. Myoma organotypic assay

The study was approved by the Ethics Committee of the Oulu University Hospital. Uterine leiomyoma tissues were obtained from routine surgeries of otherwise healthy donors after an informed consent. The freshly-dissected myoma tissue was cut into 3 mm slices and the discs were made using an 8 mm biopsy punch. Only the non-degenerated myomas were picked and discs from the same myoma (an average of 100 discs/myoma) were used in each experimental set-up. The myoma discs were stored at −70 °C in DMEM/F-12 media with 10% DMSO (Sigma-Aldrich). The cells were cultivated on top of myoma discs for 14 days as described by [23]. Briefly, the discs were put into Transwell inserts (diameter 6.5 mm, pore size 8 µm, Corning Inc., Corning, NY, USA) and the HSC-3 cells (700,000 in 50 µl) were plated on top of each disc. The cells were allowed to attach to the discs and on the next day the discs were removed from the Transwell inserts and put onto uncoated nylon mesh resting on a curved steel grid in a 12-well plate with 1 ml of medium. The media were analyzed using radioimmunoassay (RIA) to detect type III collagen degradation products, as described by [23]. After 14 days the discs were prepared for histology as described below.

To lyophilize the myoma discs they were first put onto 24-or 48-well plates, one disc per well, covered with parafilm and frozen at −70 °C. The parafilm was pierced and the discs were lyophilized for 72 h using a Heto Drywinner DW3 (Heto-Holten A/S, Allerød, Denmark). After lyophilization the discs were placed in an exicator and stored at −70 °C. The discs were rehydrated by rinsing them at 4 °C in DMEM/F-12 overnight. After rehydration the discs were used in the same manner as non-lyophilized native discs.

2.3. Scanning electron microscopy (SEM)

For SEM images (Fig. 1(A)) 700,000 HSC-3 cells were cultivated on top of myoma discs for 10 days as described above. For SEM the discs were dehydrated in an ascending ethanol series: overnight in 40%, 1 d in 50% and 3 days in 70% ethanol. To reveal the invaded cells inside the myoma, the discs were bisected. Dehydration was completed with 5 min in 80%, 5 min in 90% and twice for 5 min in 100% ethanol. After dehydration, a critical point drying was performed using a BAL-TEC Critical Point Dryer 030. Next the samples were attached to a metal platform using a two-sided carbon sticker and sputtered with a 6–12 nm platinum layer using an Agar High Solution Sputter Coater. Images were captured using Zeiss Ultra Plus field emission scanning electron microscope with 3.00 kV acceleration voltage and 8500x magnification.

2.4. Transmission electron microscopy (TEM)

For TEM images HSC-3 cells were cultivated in co-cultures with mesenchymal stem cells (400,000 of both cells, 14 days) (Fig. 1(C)) or with normal fibroblasts (400,000 of both cells, 14 days) (Fig. 1 (D)) for 10 days. Samples were cut from the top of the myoma discs and fixed in 1% glutaraldehyde 4% formaldehyde mixture in 0.1 M phosphate buffer. They were post-fixed in 1% osmium tetroxide, dehydrated in acetone and embedded in Epon LX 112 (Ladd Research Industries, Williston, Vermont, USA). Thin sections were cut with Leica Ultracut UCT ultramicrotome, stained in uranyl acetate and lead citrate and examined in Philips CM100 transmission electron microscope. Images were captured with Morada CCD camera (Olympus Soft Imaging Solutions GMBH, Munster Germany).
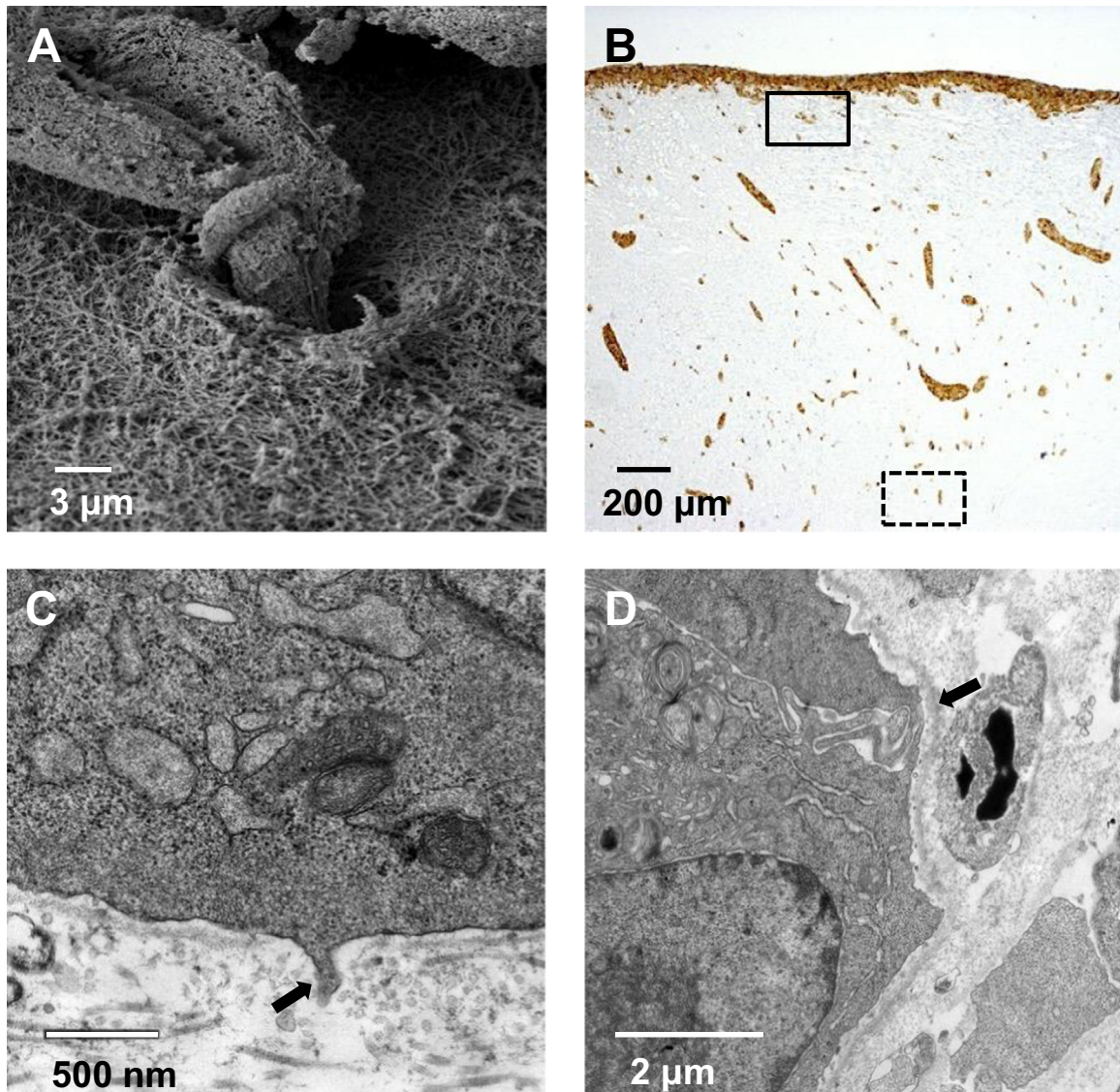
Fig. 1. HSC-3 cells invading into the myoma. A single carcinoma cell invading through bundles of collagen fibers of the myoma visualized by SEM (A). The myoma discs stored in −70 °C and used for HSC-3 invasion assays were analyzed using AE1/AE3 pancytokeratin staining (B). Myoma pieces from the upper (resting cells, D) and lower (invasive cells, C) areas were analyzed with TEM (C, D). TEM shows that the invading cells form invadopodia (C, arrow), whereas cells in the upper part of the myoma disc contained basement membrane structures surrounding the cells (D, arrow).

2.5. Heart invasion assay

The human heart sample was a kind gift from Prof. Miklós Tóth, Semmelweis University, Budapest, Hungary. Sample collection was approved by the Health and Scientific Research Ethical Committee in Budapest. The porcine heart was collected from a blood donor pig from the Laboratory Animal Centre, University of Oulu, immediately after sacrificing. The porcine heart discs were prepared from the left ventricle and were further processed as described above for the myoma organotypic culture.

Mouse and rat hearts were collected from healthy animals from the Laboratory Animal Centre, University of Oulu. The animals were sacrificed, and the hearts were removed and stored at −70 °C. When still frozen, the tissue was cut into 3 mm slices with a disposable scalpel and further into discs with a 3 mm biopsy punch. Heart discs were equilibrated in media at room temperature (RT) for one hour to prepare organotypic cultures. The heart discs were placed into Transwell inserts (CellCrown™96, diameter 3 mm; Scaffdex, Tampere, Finland) and 100,000 cells in 10 μl of media were added on top of the discs. The heart organotypic

cultures were sustained and the media was changed every 2–3 days. Collection of all animal hearts used in this study was approved by National Animal Experiment Board in Finland (ELLA).

2.6. Porcine tongue organotypic assays

The healthy porcine tongues were collected from the Laboratory Animal Centre, University of Oulu, immediately after sacrificing the pig that had been used by another research group who studied bone marrow mononuclear cell migration to ischemic brain tissue [19]. Their study was approved by the Research Animal Care and Use Committee of the University of Oulu. Tongues were stored at −70 °C. The tongues were first sterilized by dipping for 5 seconds in 70% ethanol followed by shaping the discs with an 8 mm biopsy punch from the lateral border of the tongues (Fig. 2 (C)). The experiments with tongue discs were modified in three different ways. The discs were stored either overnight at 4 °C, or in an incubator (37 °C, 5% CO$_2$), or they were taken straight from the freezer (−70 °C) and thawed just before the invasion assay was started. The process is illustrated in Fig. 2. The tongue discs were
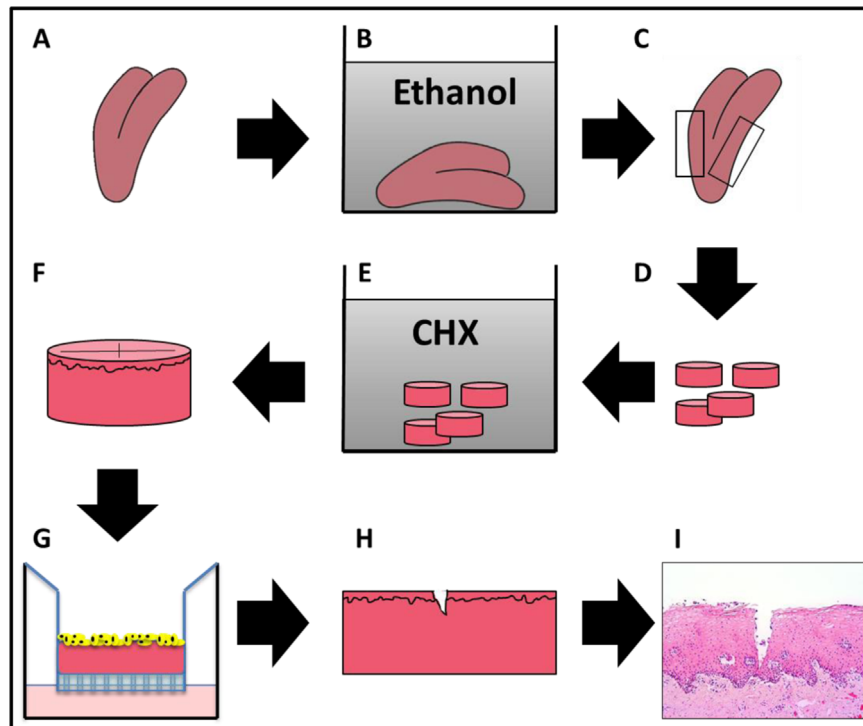
Fig. 2. Schematic drawing of the tongue model protocol. (A) Porcine tongues were harvested from animals sacrificed for other experimental set-ups. (B) The tongues were sterilized by dipping them into 70% ethanol for 5 s (C) Lateral sides from the anterior two thirds of the tongue were dissected. D) An 8 mm biopsy punch was used to make discs from cut off lateral sides of the tongues. (E) Discs were sterilized by rinsing them in chlorhexidine (CHX) solution for 5 min. (F) X-shaped cuts were made with a disposable scalpel to break the epithelium of the discs. (G) Discs were placed in Transwell inserts and cells were added on top of the discs. The discs were incubated for 11 days followed by formalin fixation and paraffin embedding. (H) 5 μm thick slices were cut and HE stained. (I) HE stained section of the tongue showing the cut line on the epithelial surface.

rinsed then in 0.2% chlorhexidine gluconate for 5 min (GlaxoSmithKline Oy, Corsodyl, chlorhexidine gluconate 2 mg/ml, Consumer Healthcare, Espoo) and the epithelium of the tongue was injured using either the tip of a plastic pipette to create small scratches, sharp tipped tweezers to create wounds or surgical knife to make X-shaped cuts through the keratinized epithelial surface. After punching the discs, they were transferred into Transwell inserts and DMEM/F-12 cell culture medium containing complete serum (600 μl) was added into the lower compartment and cells (200,000 in 50 μl) were added on top of the discs. Media were changed daily during the 9–11 days of incubation. After the incubation the discs were fixed in 4% formalin (24 h). The preparation of histological sections and immunohistology is described below.

2.7. Invasion assay with HSC-3 and CAFs or NOFs

HSC-3 cells (200,000 in 50 μl) were applied on top of myoma or tongue discs (with cuts as described above) with or without CAFs or NOFs (200,000 in 50 μl). All cells were fluorescently labeled with lipophilic long-chain dialkylcarbocyanine stains, HSC-3 cells with green (DiO) and CAFs/NOFs with red dye (DiI) (Vybrant labels, Invitrogen). Normal DMEM/F-12 media and myoma RM were used for tongue discs and only normal medium for myoma discs. The incubation time was 11 days. The sections were DAPI stained and photographed using an AMG EVOS$_{fl}$ microscope system.

2.8. Histology and immunohistochemistry

The organotypic cultures were fixed at day 14 (day 9 or 11 for porcine tongue assays) in 4% neutral-buffered formalin overnight. The samples were dehydrated, bisected and embedded in paraffin. 6 μm sections were deparaffinized and stained with Mayer's HE.

The endogenous peroxidase activity was blocked with H_2O_2 in MeOH for 30 min for pancytokeratin AE1/AE3 (Dako) staining. Antigen retrieval was performed by 0.4% pepsin in 0.01 M HCl at 37 °C for 20 min. Sections were blocked in 2% bovine serum albumin (BSA)/PBS for 30 min and incubated with primary antibodies in a humidified chamber at 37 °C for 30 min and at 4 °C overnight. Dilution (1:150) was prepared in REAL Antibody diluent (Dako). Biotinylated secondary antibody anti-mouse was applied for 1 h and StreptABComplex/horseradish peroxidase (HRP, Dako) in 0.5 M NaCl/PBS was applied for 30 min. Between each step the sections were washed twice in PBS for 10 min.

Myomas were stained for tenascin-C (TNC) as follows: for epitope retrieval, the sections were heated in a microwave oven in Tris-EDTA solution (pH 9) for 10 min and allowed to cool down at RT for 20 min Endogenous peroxidase activity was blocked using DAKO Peroxidase-blocking solution S2023 for 10 min The sections were then incubated with primary antibody (DB7, order #610003, Biohit, Helsinki, Finland) at a dilution of 1:500 for 60 min at RT. For visualization, HRP was introduced to the slides for 10 min, after which DAB chromogen was used for 5 min, the sections were counterstained using Mayer HE for 1 min and mounted mechanically. No quantifications were performed from TNC stained myoma sections.

Myoma and heart organotypic assays performed with G-361 cells were stained with S100. The antigen retrieval was performed by 0.4% pepsin in 0.01 M HCl at 37 °C for 30 min. The sections were incubated overnight at 4 °C with polyclonal rabbit anti-human S100 antibody (Dako Z0311, 1:3000).

From stained sections, the maximum invasion depth and/or area of invaded cells were quantified as described by [23].

2.9. Radioimmunoassay

A type III collagen C-terminal peptide (IIICTP) radio-immunoassay was used to investigate if invading cells degraded type III collagen when invading the ECM of tissue discs. Polyclonal antibody against IIICTP was raised in rabbits [22]. The IIICTP antigen was a synthetic peptide SP99 (NeoMPS). The synthetic peptide was conjugated to bovine thyroglobulin with carbodiimide (EDC; Pierce), according to the manufacturer's instructions. The dialyzed conjugate was emulsified with 0.9% NaCl and Freunds adjuvant (Sigma) and injected subcutaneously into rabbits at three- to four-week intervals.

Polyclonal antiserum for SP99 was diluted for IIICTP-RIA. SP99 was labeled by the Chloramine-T method using ^{125}I [29]. An extra tyrosine was added to the C-terminus of SP99 to facilitate radio-iodination. To create a standard curve, serial dilutions of SP99 were used. 100 μl of tissue sample media were incubated with 200 μl of the antiserum dilution and 200 μl of ^{125}I-SP99 solution at 37 °C for 2 h. Next 500 μl of the secondary goat anti-rabbit antibody (200 μg/ml, Fitzgerald) in 15% polyethylene glycol (6 kDa) was added and the samples were incubated at 4 °C for 30 min The samples were centrifuged at $2000 \times g$ at 4 °C for 30 min after which the radioactivity of the precipitates was measured with a gamma counter (Wizard 1470; Wallac).

2.10. Gel filtration chromatography and wound healing assay

Aliquots of the heart tissue RM (3.5 ml) and myoma tissue RM (13 ml) were lyophilized. The dry residues were each re-dissolved in 3 ml of 0.1 M ammonium acetate (pH 6), and applied separately to a Sephadex G-75 gel filtration column (2.5×28 cm^2) and eluted with the same buffer at 54 ml/h. Fractions of 9 ml were collected. The absorbance at 280 nm was measured using a Nanodrop spectrophotometer (Thermo Scientific). The effect on cell migration was tested by pooling the aliquots from three adjacent fractions (5–7, 8–10, 11–13, 14–16, and 17–19). The test samples were lyophilized, redissolved in the cell culture medium and their effect on cell migration was studied in a wound healing assay as described [31]. Briefly, HSC-3 cells were grown to confluency, wounds were created with a 1 ml pipette tip and the wound closure was monitored. The wound healing rate was determined as a comparison of initial wound area to the wound area after 20 h of cultivation.

2.11. Mass spectrometry

The protein content of myoma RM was assessed using mass spectrometry. First, six myoma discs were rinsed for 24 h. Next the rinsing media were combined into two pools each containing rinsing media from three myomas. Mass spectrometry analysis was performed for both pools.

The rinsing media were concentrated using a 3 kDa centrifugal filter (Amicon Ultra, Millipore, Ireland) at 4 °C, and the proteins were treated with a final concentration of 1.6 M urea. The samples were reduced (5 mM dithiothreitol, 25 min at 56 °C), alkylated (14 mM iodoacetamide, 30 min at RT in the dark) and digested with trypsin (1:50, w/w). The reaction was stopped with 1% trifluoroacetic acid and desalted with Sep-pack cartridges. The samples were dried in a vacuum concentrator, reconstituted in 0.1% formic acid and analyzed by LC-MS/MS. Two independent experiments were performed.

An aliquot containing 3 μg of proteins was analyzed on an electron-transfer dissociation enabled LTQ Orbitrap Velos Mass Spectrometer (Thermo Fisher Scientific, USA) connected to a na-noflow liquid chromatography column (LC-MS/MS) by an EASY-nLC System (Proxeon Biosystem) through a proxeon nanoelectrospray ion source. Peptides were separated by a 2–90% acetonitrile gradient in an analytical PicoFrit column (20 cm × id 75 μm, 5 μm particle size, New Objective) at a flow of 300 nl/min over 212 min The nanoelectrospray voltage was set to 2.2 kV, and the source temperature was 275 °C. All instrumental methods for the LTQ Orbitrap Velos were set up in the data-dependent analysis mode. The full scan MS spectra (m/z 300–1600) were acquired in the Orbitrap analyzer after accumulation to a target value of 1e^6. The resolution in the Orbitrap was set to r=60000. The 20 most intense peptide ions with charge states ≥ 2 were sequentially isolated to a target value of 5000 and fragmented in the linear ion trap by low-energy collision-induced dissociation (normalized collision energy of 35%). The signal threshold for triggering an MS/MS event was set to 1000 counts. Dynamic exclusion was enabled with an exclusion size list of 500, an exclusion duration of 60 s, and a repeat count of 1. An activation q=0.25 and an activation time of 10 ms were used.

The raw files were processed using the MaxQuant version 1.2.7.429 and the MS/MS spectra were searched using the Andromeda search engine against the Uniprot Human Protein Database (release July 11, 2012; 69,711 entries). The initial maximal allowed mass tolerance was set to 20 ppm for precursor and then set to 6 ppm in the main search and to 0.5 Da for fragment ions. Enzyme specificity was set to trypsin with a maximum of two missed cleavages. Carbamidomethylation of cysteine (57.021464 Da) was set as a fixed modification, and oxidation of methionine (15.994915 Da) and protein N-terminal acetylation (42.010565 Da) were selected as variable modifications. The minimum peptide length was set to 6 amino acids. Label-free protein quantification was performed using a previously described label-free quantification (LFQ) algorithm implemented in the MaxQuant software with a 2 min window for matching between runs and maximum 1% peptide and 1% protein false discovery rate (Cox & Mann 2008). Protein intensity values were normalized using the LFQ algorithm available through the MaxQuant program and used to further identify differentially expressed proteins. Bio information analyses of the data were performed using Perseus v.1.2.7.4 software. Reverse and "only identified by site" entries were excluded. LFQ intensity values were log2 transformed; the dataset was filtered by two minimum valid values in at least one group, and statistical significance was assessed by applying Student's t-test to identify differentially expressed proteins.

2.12. Statistical analysis

Data were analyzed with independent samples t-test (IBM SPSS Statistics version 21) and results were considered to be statistically significant if the p-value was lower than 0.05. P-values are represented in figures as *$p \leq 0.05$, **$p \leq 0.01$ and ***$p \leq 0.001$. In boxplots the median is marked with a horizontal line, mean with square, the box representing 25–75% percentiles and whiskers representing standard deviation.

3. Results

3.1. Invading and dormant carcinoma cells feature distinct cell membrane structures

HSC-3 cancer cell invasion into the uterus leiomyoma organotypic model was visualized using SEM (Fig. 1(A)) followed by immunohistochemistry with cytokeratin AE1/AE3-staining (Fig. 1(B)) and TEM (Fig. 1(C) and (D)). Carcinoma cells in the invasion front (dotted rectangle in 1B) featured invadopodia structures (Fig. 1(C), arrow), whereas in the upper part of the disc (solid rectangle in 1B), the non-invasive cells were mostly surrounded by basement
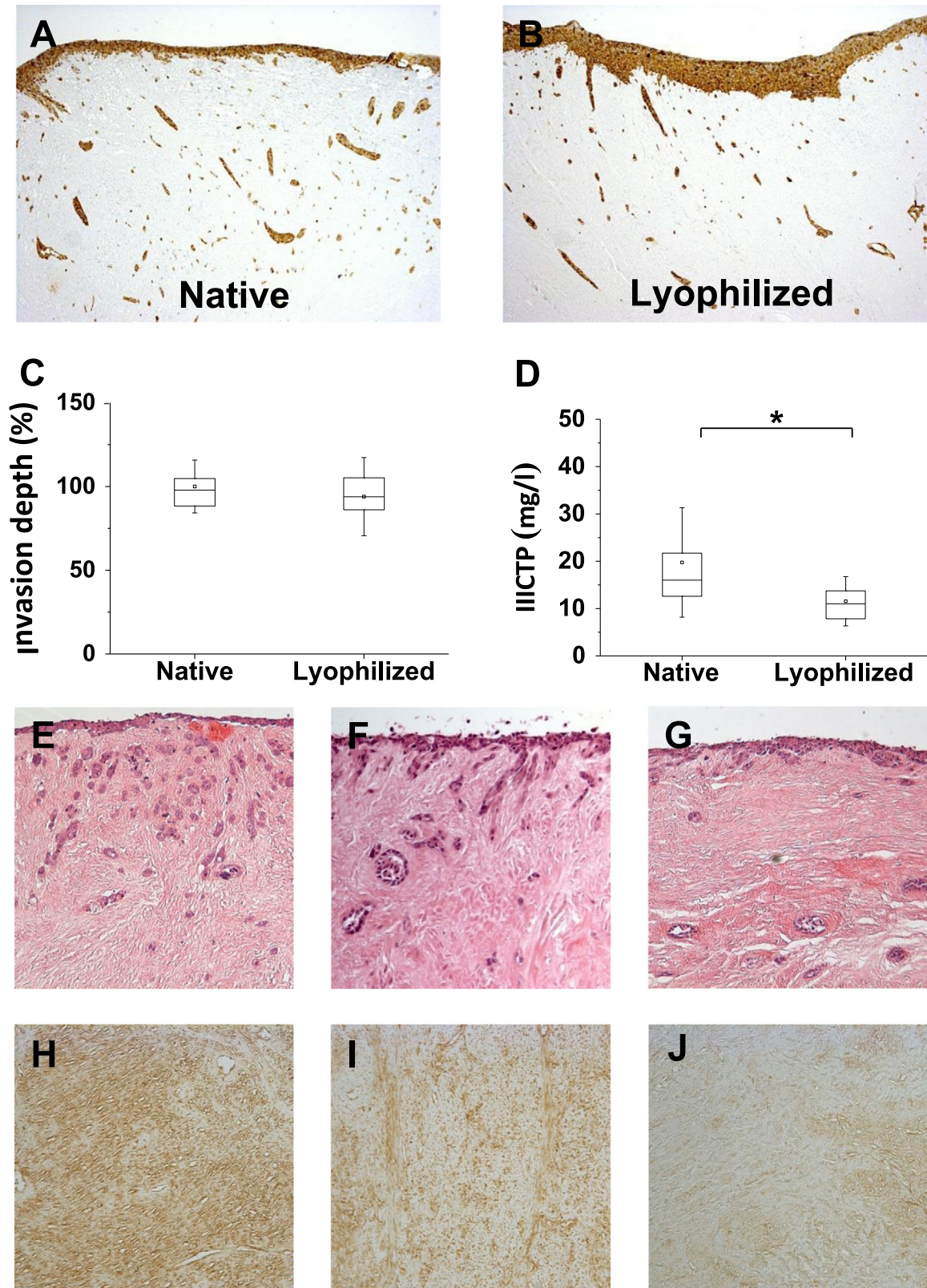
Fig. 3. HSC-3 cell invasion assay using native (A) and lyophilized (B) myoma discs. Invasion depths were analyzed from AE1/AE3 stained sections of native (n=26) and lyophilized (n=19) myoma discs (C). Carboxy-terminal peptide of type III collagen (IIICTP) concentrations (which indicate type III collagen degradation) were analyzed using RIA from native (n=9) and lyophilized (n=12) myoma discs (D). HE staining of HSC-3 cells invading in various myoma discs from different patients (E - G) shows variation in invasion efficiencies between different types of patient samples. There is vast variation in the amount of tenascin-C in the matrix of different types of myomas from abundant (H) to scanty (J). *p ≤ 0.05.

membrane structures (Fig. 1(D), arrow).

3.2. Lyophilization of the myoma model affects collagen degradation, but not the invasion pattern

We then tested if the HSC-3 invasion assay results from frozen native discs (Fig. 3(A)) could be recapitulated using lyophilized and rehydrated myoma discs (Fig. 3(B)). Based on the invasion depth analysis, no difference was found between the native or lyophilized discs (Fig. 3(C)). However, there was a statistically significant difference in IIICTP levels between lyophilized (11.6 mg/l) and native (19.8 mg/l) myoma assays, which indicates that the HSC-3 cells invading in lyophilized and rehydrated discs degraded

less type III collagen than in native discs (Fig. 3(D)). However, it is important to note that although there were no differences in the pattern or depth of invasion between the native and lyophilized discs prepared from the same myoma samples, the mainly budding pattern of HSC-3 invasion (as well as SCC-15 and SCC-25, not shown) varied between discs from different patients (Fig. 3(E)–G). Therefore, different myomas should not be combined in one experimental set-up. Additionally, we recommend that every myoma for invasion assays should first be pretested – *e.g.* using "standard" HSC-3 carcinoma cells - to discard those myomas that have unusual invasion inductive properties. The variation of invasion efficiencies between myomas might partially be due to differences in invasion inductive matrix composition, such as the amount of TNC
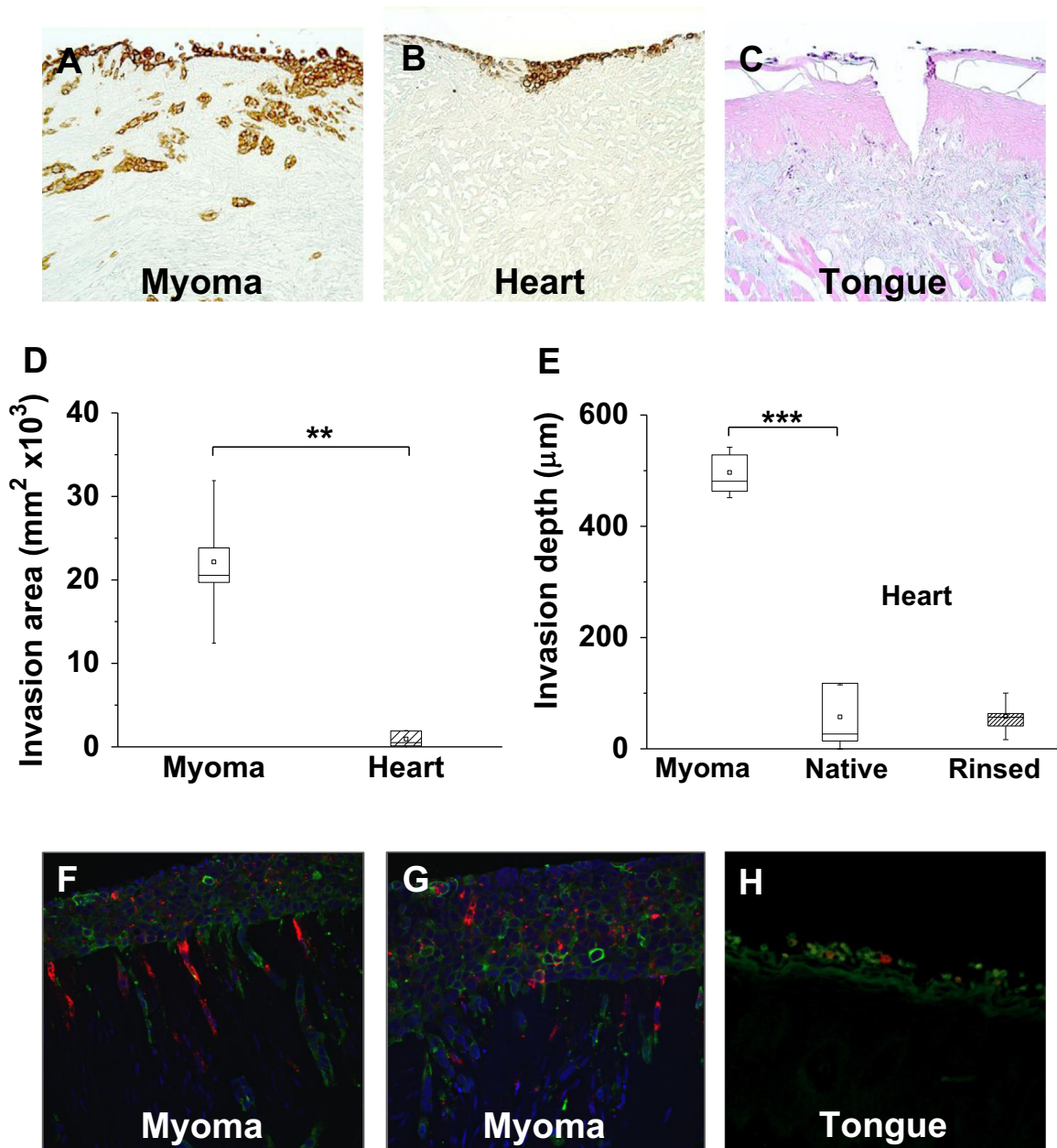

Fig. 4. **HSC-3 invasion assays using different types of tissues.** HSC-3 cells were cultivated on top of myoma (A), human heart (B) and porcine tongue (C) discs after which the myoma and heart discs were prepared for immunohistological staining. Tongue discs were HE stained. The experiment was performed also using rinsed heart (n=9) discs. The invasion area (D) and depth (E) were measured from stained sections. There was no detectable invasion in tongue discs (C and H). Invasion in heart discs was barely detectable (B, D and E), and invasion area and depth were considerably larger in native myoma discs (n=5) compared to native heart discs (n=13) (D and E). CAFs (F, red) and NOFs (G, red) were cultivated on top of the myoma discs (F and G) in co-cultures with HSC-3 cells (green). CAFs and HSC-3 cells were also cultivated on tongue discs (H), where no invasion was detected. $*p \leq 0.01$ and $***p \leq 0.001$. (For interpretation of the references to color in this figure legend, the reader is referred to the web version of this article.)

(Fig. 3(H)–J).

3.3. Heart or tongue tissues do not attract HSC-3 invasion

Using the highly invasive HSC-3 cell line we next tested if cancer cells are able to invade into healthy human heart tissue discs (Fig. 4(B)) as readily as they invade into myoma tissue (Fig. 4 (A)). Native myoma, and native and rinsed heart discs were used in this experiment. We found that there was only minimal invasion into the human heart matrix both in native and rinsed discs (Fig. 4

(B), D and E) and there was no invasion in mouse, rat or porcine heart tissue discs (not shown). Invasion depth and area in myoma were vastly larger compared to those in the heart (Fig. 4(D) and (E)). Since HSC-3 is an aggressive tongue carcinoma cell line, we also tested whether HSC-3 cells could invade into their "natural matrix", healthy tongue discs (Fig. 2). Although HSC-3 cells invaded into myoma, they showed hardly any penetration into the tongue discs (Fig. 4(C)), even after the surface was wounded as described before (Figs. 2 and 4(C)). The tongue discs were not invaded (Fig. 4(H)) even after co-culturing HSC-3 cells (green) with
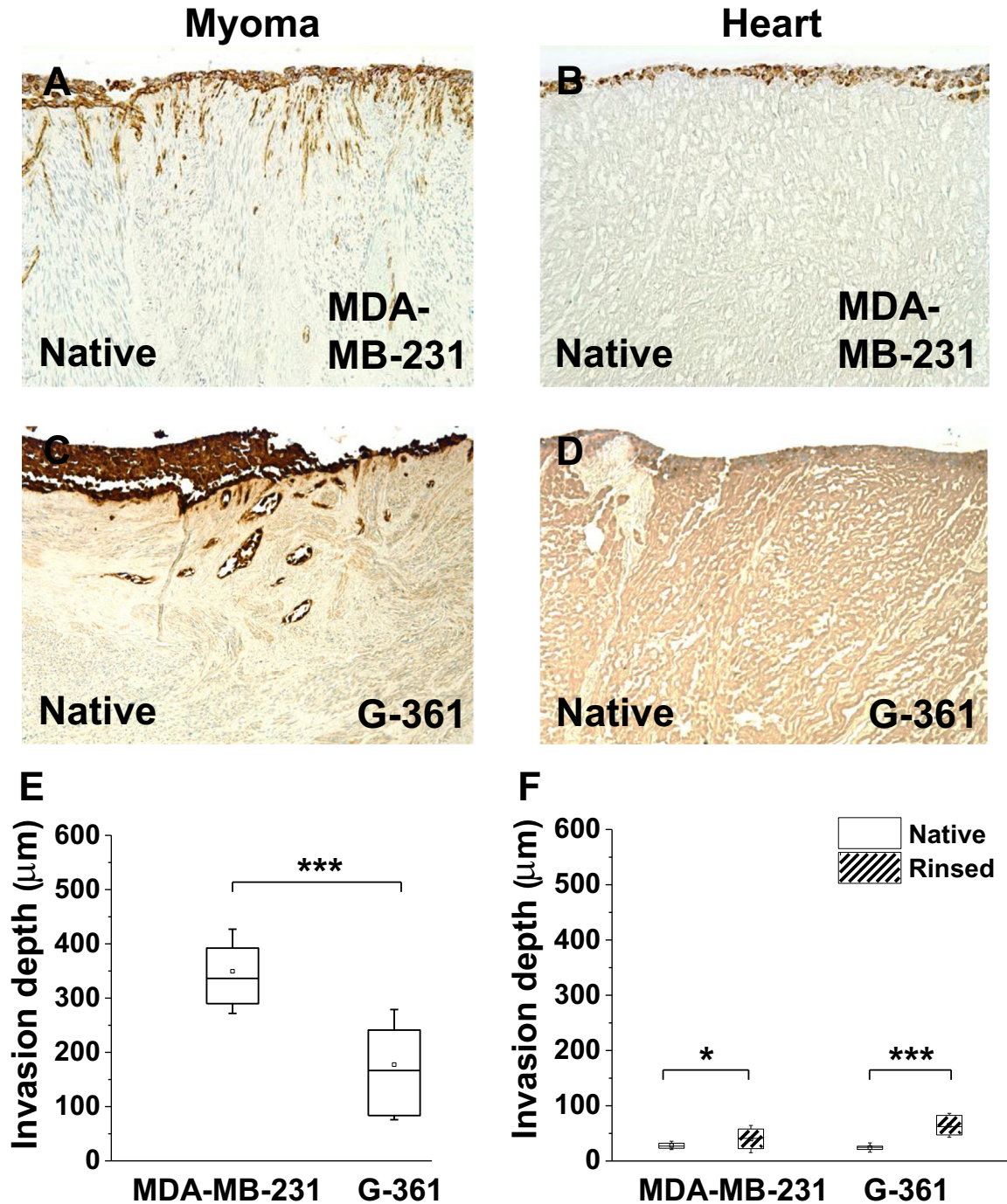

Fig. 5. **The effect of soluble factors on malignant cell invasion into human heart.** Heart tissue discs, with or without the rinse period of 3 days, and native myoma discs were used in the invasion assays. Ductal breast adenocarcinoma cells (MDA-MB-231, A and B) and malignant melanoma cells (G-361, C and D) were cultivated on top of myoma (A and C) and heart discs (B and D) for 14 days. In myoma discs, the invasion depth of MDA-MB-231 cells ($n=8$) was significantly greater compared to G-361 cells ($n=14$) (E). In the heart, rinsing the discs increased the invasion depth of MDA-MB-231 ($n=13$ for native and 10 for rinsed) cells and G-361 cells ($n=8$ for native and 11 for rinsed) cells (F). *$p \leq 0.05$ and ***$p \leq 0.001$.

CAFs or NOFs (red), unlike in myoma discs (Fig. 4(F) and (G)).

3.4. Breast carcinoma and melanoma cells invade more in rinsed heart matrix

Since the invasion efficiency of the HSC-3 cell line clearly differed between myoma and heart tissue discs, we tested other invasive cell lines in these matrices as well. The invasion of breast carcinoma MDA-MB-231 (Fig. 5(A) and (B)) and melanoma G-361 (Fig. 5(C) and (D)) cells in native myoma, and native and rinsed hearts was analyzed. In myoma, deeper invasion was detected using MDA-MB-231 cells in comparison to G-361 cells (Fig. 5(E)). Similar to HSC-3 cells, the breast carcinoma and melanoma cell lines showed poor invasion into the native solid matrix of the heart tissue (Fig. 4(D) and (E); Fig. 5(F)), but the invasion of all cell lines was slightly induced after rinsing off the soluble fraction of the heart matrix.

3.5. Heart tissue contains migration inhibiting factors

Next we analyzed the gel filtration fractions of human heart and myoma RM using wound healing scratch assays. We found that small molecular weight fractions from the heart rinsing media caused marked inhibition of HSC-3 migration compared to the similar size fractions from the myoma rinsing media (Fig. 6(A) and (B)). This suggests that the heart tissue contains soluble factors that are able to inhibit cancer cell migration, which most likely affects invasion as well.

3.6. Myoma tissue contains growth factors as well as their receptors and binding proteins

Since we have previously shown that rinsing myoma discs decreases invasion depth and increases type III collagen degradation [31], we wanted to elucidate the mechanisms of this effect and analyzed the protein content of the myoma rinse. In the myoma rinse we found a variety of growth factors as well as their receptors and binding proteins (Table 1), including various migration affecting growth factors, such as fibroblast growth factor 2 (FGF2), transforming growth factor beta (TGF-β) 1 and −2 and hepatocyte growth factor (HGF).

4. Discussion

Our group has developed a three-dimensional organotypic invasion assay based on human uterine leiomyoma tissue [23]. Here we found that the myoma discs also function in invasion assays after lyophilization and rehydration, which makes their utilization and shipment more straightforward. On the other hand, healthy human heart or porcine tongue discs did not induce invasion, and rinsing of the heart discs to remove soluble factors resulted in only a slight induction of invasion. Moreover, the small molecular weight molecules from human heart rinsing media inhibited cancer cell migration. These results demonstrate that non-neoplastic healthy tissue is less able to induce invasion, and furthermore that the migration inhibitory effects of heart tissue may partially be due to soluble factors released from the tissue.

The composition of TME in cancerous tissue, for example the presence of ECM molecules, cytokines and proteases, could include highly important predictors of cancer prognosis. ECM may limit cancer initiation at early stages, whereas after modification by cancer cells at later stages, it can drive tumor progression [26]. We have shown that depleting soluble factors by rinsing the myoma discs alters the invasion efficacy and pattern of aggressive oral cancer cells [31]. Here we demonstrated that, similar to rinsed
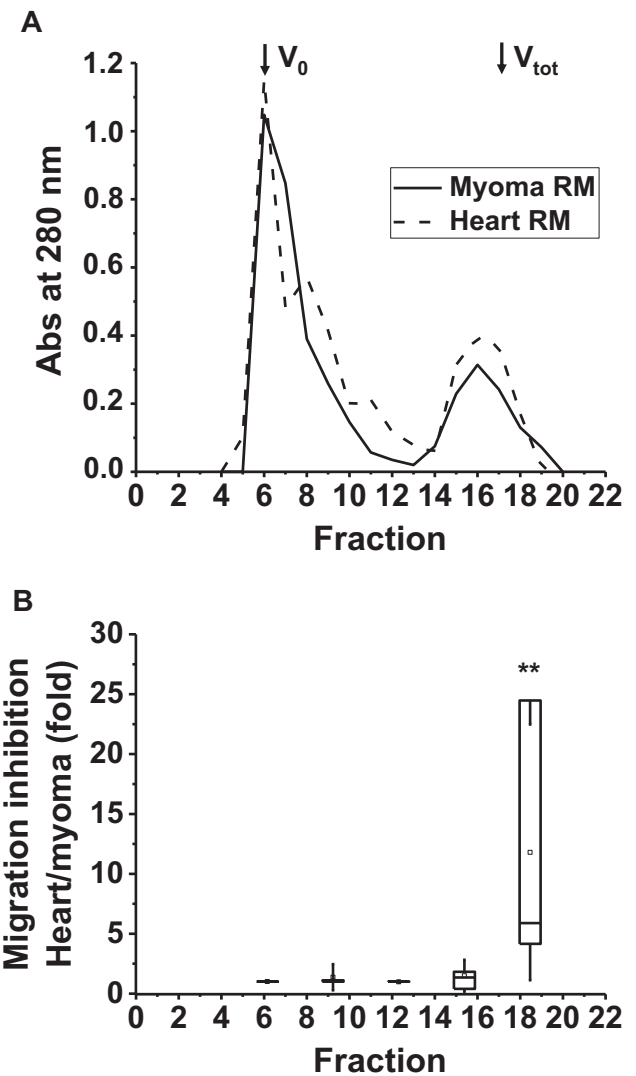
Fig. 6. Fractions of human heart and myoma rinsing media have distinct effects on HSC-3 cell migration. Two identical runs were performed. The small molecular weight fractions (Sephadex G-75 gel filtration fractions 17–19) (A) from the heart rinsing media (RM) caused a marked inhibition of the cell migration compared to the similar fractions from the myoma RM (B). The lines denote absorbance at 280 nm measured from the fractions (solid line, myoma RM; dashed line, heart RM) (A). The boxes (n=6 for each box) denote the ratio of migration inhibition of heart washings to that of the myoma washings (B). Identical pooled fractions (5–7, 8–10, 11–13, 14–16, and 17–19) from the two gel filtration runs were tested. The response to the pure cell culture medium was set to 1. V_0, void volume; V_{tot}, total volume of the column. **$p \leq 0.01$.

myomas [31], invading HSC-3 cells degraded type III collagen more efficiently in native than in lyophilized and rehydrated myoma discs. This indicates that lyophilization and rehydration alters the matrix structures and may allow cancer cells to invade the tissue with less need to degrade the collagen fibers. However, although the invasion mechanisms varied between native and lyophilized myoma matrix, there was no difference in invasion depth, which indicates that lyophilized myoma tissue could be utilized in invasion assays as well as native myoma.

Primary malignancies of the heart are extremely uncommon. Although primary cardiac tumors are rare, tumors that metastasize to the heart from other organs occur more commonly. These secondary tumors have an incidence of 1.23% in autopsy reports [16]. The most common tumors with cardiac metastatic potential are carcinomas of the lung, breast and esophagus, but also lymphoma, leukemia and melanoma cells have been found to metastasize to

Table 1
The most abundant proteins identified from myoma rinsing media using mass spectrometry. Proteins included growth factors, and their binding proteins and receptors. The gene coding the protein, name of the protein, top enriched biological process and cellular component are listed.

Gene	Protein	Top enriched BP	Cellular component
Binding proteins			
IGFBP3	Insulin-like growth factor-binding protein 3	Apoptotic process	Extracellular
GRB2	Growth factor receptor-bound protein 2	Modulation by virus of host morphology or physiology	Plasma membrane
FGFBP1	Fibroblast growth factor-binding protein 1	Negative Regulation of cell proliferation	Extracellular
IGFBP7	Insulin-like growth factor-binding protein 7	Negative regulation of cell proliferation	Extracellular
IGFBP5	Insulin-like growth factor-binding protein 5	Signal transduction	Extracellular
HDGFRP2	Hepatoma-derived growth factor-related protein 2	Transcription, DNA-dependent	Nucleus
LTBP3	Latent-transforming growth factor beta-binding protein 3	Transforming growth factor beta receptor signaling pathway	Extracellular
LTBP4	Latent-transforming growth factor beta-binding protein 4	Transforming growth factor beta receptor signaling pathway	Extracellular
Growth factors			
FGF2	Fibroblast growth factor 2	Apoptotic process	Extracellular
TGFB2	Transforming growth factor beta-2	Axon guidance	Extracellular
HDGF	Hepatoma-derived growth factor	Cell proliferation	Extracellular
PDGFB	Platelet-derived growth factor subunit B	Negative regulation of transcription, DNA-dependent	Extracellular
PDGFA	Platelet-derived growth factor subunit A	Platelet activation	Extracellular
EGF	Pro-epidermal growth factor	Platelet activation	Extracellular
GDF9	Growth/differentiation factor 9	Positive regulation of cell proliferation	Extracellular
TGFB1	Transforming growth factor beta-1	Positive regulation of transcription from RNA polymerase II promoter	Extracellular
VEGFA	Vascular endothelial growth factor A	Positive regulation of transcription from RNA polymerase II promoter	Extracellular
IGF1	Insulin-like growth factor I	Positive regulation of transcription from RNA polymerase II promoter	Extracellular
HGF	Hepatocyte growth factor	Positive regulation of transcription from RNA polymerase II promoter	Extracellular
TGFB1I1	Transforming growth factor beta-1-induced transcript 1 protein	Positive regulation of transcription, DNA-dependent	Nucleus
IGF2	Insulin-like growth factor II	Regulation of transcription, DNA-dependent	Extracellular
CTGF	Connective tissue growth factor	Small molecule metabolic process	Extracellular
Receptors			
TGFBR2	TGF-beta receptor type-2	Apoptotic process	Plasma membrane
FGFR3	Fibroblast growth factor receptor 3	Apoptotic process	Plasma membrane
FGFR2	Fibroblast growth factor receptor 2	Apoptotic process	Extracellular
NTRK1	High affinity nerve growth factor receptor	Axon guidance	Plasma membrane
EPS15	Epidermal growth factor receptor substrate 15	Cell proliferation	Plasma membrane
IGF1R	Insulin-like growth factor 1 receptor	Immune response	Plasma membrane
PDGFRA	Platelet-derived growth factor receptor alpha	Modulation by virus of host morphology or physiology	Plasma membrane
KDR	Vascular endothelial growth factor receptor 2	Modulation by virus of host morphology or physiology	Extracellular
EGFR	Epidermal growth factor receptor	Negative regulation of apoptotic process	Extracellular
FRS2	Fibroblast growth factor receptor substrate 2	Neurotrophin TRK receptor signaling pathway	Plasma membrane
MET	Hepatocyte growth factor receptor	Positive regulation of transcription from RNA polymerase II promoter	Extracellular
FGFR1	Fibroblast growth factor receptor 1	Transcription, DNA-dependent	Extracellular

the heart [9,28]. Carcinoma cells metastasize into the epicardium preferably via a lymphatic route while many tumors, especially lymphoma and melanoma, can invade into the myocardium via a hematogenous route [17,28]. It is speculated that intracavitary pressure, high blood flow and contractile strength may protect the heart from metastatic invasion [9]. Obviously, the heart ECM around the striated muscle myocytes also differs from most other tissue matrices, and may explain why cancer cells do not invade into it.

We showed that in addition to the HSC-3 cells, also the metastatic breast cancer or malignant melanoma cell lines did not invade into the heart tissue discs. Invasion of cancer cell lines through myoma tissue can be seen via existing vessels within the myoma matrix. However, the vessels of human heart discs were not utilized for invasion. We demonstrated that one explanation for this anti-invasive effect could be the presence of soluble inhibitory factors within the heart tissue. Especially in the case of malignant melanoma cells, rinsing off the soluble compounds enhanced the cell invasion. However, even then the depth of invasion of melanoma cells was not at the same level as in myoma

discs. In the case of breast and tongue cancer the invasion was also increased in rinsed discs, but the differences were less obvious. This indicates that heart tissue has inhibitory fractions that affect cell invasion. In fact, in a migration assay, small molecular weight fractions from heart rinsing media significantly inhibited the migration of the HSC-3 cell line. The identification of these soluble inhibitory factors and their effects on various cancer cell lines are exciting topics for further studies.

In the invasion assays, the most "natural TME" for HSC-3 cells, the porcine tongue tissue, was unable to induce their invasion. Even after adding myoma disc rinsing media as chemoattractant, invasion into the tongue was not induced. We then tested whether CAFs could enhance invasion induction into tongue discs. CAFs are known to have a role in carcinoma invasion _in vivo_ by causing so called "fibroblast-led collective invasion" [12]. CAFs form the leading edge of invading cells (Fig. 4(F)) and make a path for carcinoma cells to follow, as well as serve as a prognostic indicator in oral squamous cell carcinoma (OSCC) [7]. We added CAFs together with HSC-3 cells on top of myoma and tongue discs. Although HSC-3 cells invaded myoma as expected, the addition of

CAFs did not induce invasion of tongue discs. In addition, bone marrow mesenchymal stem cells that we have shown to be able to induce HSC-3 invasion in myoma [30] were not able to induce HSC-3 invasion into the tongue tissue discs. This may be due to species differences (human myoma *versus* porcine tongue). Most likely, however, it is because myoma, unlike healthy tongue, presents an ECM that mimics the tumor microenvironment phenotype. This tumor ECM differs from that of healthy tissue in that it contains *e.g.* more laminins, type IV collagen, lysyl-oxidase-1 (LOX-1) [23,31] and tenascin-C, as shown here in the myoma matrix (Fig. 3(H)–J).

Finally, in order to elucidate the previously detected decrease in invasion depth and increase in collagen degradation in rinsed myoma matrix [31], we deprived myoma tissue of its soluble factors by rinsing and analyzed the rinsing media utilizing mass spectrometry. This revealed a variety of growth factors as well as their binding proteins and receptors (Table 1). Some of these growth factors are known for their migration enhancing nature, including FGF2, TGF-β1 and −2 and HGF. Of these growth factors, TGF-β1 and HGF are of special interest, since TGF-β1 induced myofibroblasts are shown to secrete HGF that increases invasion of OSCC cells *in vitro* [6,18]. Additionally, TGF-β1 induces an epithelial-mesenchymal transition (EMT) in OSCC cells, a process in which cells of epithelial origin gain properties of mesenchymal cells, including loss of adhesion and increased migratory capabilities [25]. Some of the changes between invasion in native and rinsed myomas detected previously [31] could be attributed to these migration and invasion increasing growth factors in myoma rinsing media. However, as we have established, individual myomas vary in terms of composition and invasion aiding capabilities. Hence it cannot be deduced that all myomas contain these same growth factors in similar proportions. This variation in proportions of growth factors could lead to different responses in cells invading into the myoma, a complexity known also from different types of cancers. An excellent example of this complexity is TGF-β, which was prominent in myoma rinsing media; it possesses both pro- and anti-tumorigenic features depending on the state of both the microenvironment and the cancer cells [20]. The varying interactions of cancer cells with soluble and insoluble factors of TME remain a topic for further studies. What are the cumulative interactions leading to enhancement or inhibition of invasion, and could new treatments be generated to modulate these interactions?

In conclusion, the importance of TME in carcinogenesis is well recognized. This provides the rationale behind the use of human tumor-derived matrix for cancer invasion studies rather than rodent or synthetic tumor matrices. Myoma is therefore an ideal tool to obtain answers of the co-operative behavior of the cells in the complex TME mimicking tumor matrix. However, myomas of single origin should be used in each experimental set-up. As demonstrated here, neither the healthy human tissue discs nor healthy porcine, mouse or rat tissue, either tongue or heart, supported invasive cancer growth. Furthermore, we demonstrated that soluble factors from human heart inhibited cancer migration and invasion *in vitro*. These so far uncharacterized factors may also partially explain why primary tumors or metastases rarely invade into the human heart.

References

[1] M. Agostini, L.Y. Almeida, D.C. Bastos, R.M. Ortega, F.S. Moreira, F. Seguin, K.G. Zecchin, H.F. Raposo, H.C.F. Oliveira, N.D. Amoêdo, T. Salo, R.D. Coletta, E. Graner, The fatty acid synthase inhibitor orlistat reduces the growth and metastasis of orthotopic tongue oral squamous cell carcinomas, Mol. Cancer Ther. 13 (3) (2014) 585–595, http://dx.doi.org/10.1158/1535–7163.MCT-12–1136.

[2] I. Alahuhta, M. Aikio, O. Väyrynen, S. Nurmenniemi, J. Suojanen, S. Teppo, T. Pihlajaniemi, R. Heljasvaara, T. Salo, P. Nyberg, Endostatin induces proliferation of oral carcinoma cells but its effect on invasion is modified by the tumor microenvironment, Exp. Cell Res. 336 (1) (2015) 130–140, http://dx.doi.org/10.1016/j.yexcr.2015.06.012.

[3] M. Allen, J. Louise Jones, Jekyll and Hyde: the role of the microenvironment on the progression of cancer, J. Pathol. 223 (2) (2011) 162–176, http://dx.doi.org/10.1002/path.2803.

[4] A. Almangush, I.O. Bello, H. Keski-Säntti, L.K. Mäkinen, J.H. Kauppila, M. Pukkila, J. Hagström, J. Laranne, S. Tommola, O. Nieminen, Y. Soini, V.-M. Kosma, P. Koivunen, R. Grénman, I. Leivo, T. Salo, Depth of invasion, tumor budding, and worst pattern of invasion: prognostic indicators in early-stage oral tongue cancer, Head Neck 36 (6) (2014) 811–818, http://dx.doi.org/10.1002/hed.23380.

[5] P. Åström, E. Pirilä, R. Lithovius, H. Heikkola, J.T. Korpi, M. Hernández, T. Sorsa, T. Salo, Matrix metalloproteinase-8 regulates transforming growth factor-ß1 levels in mouse tongue wounds and fibroblasts *in vitro*, Exp. Cell Res. 328 (1) (2014) 217–227, http://dx.doi.org/10.1016/j.yexcr.2014.07.010.

[6] P.J. Barth, T.S. Zu Schweinsberg, A. Ramaswamy, R. Moll, CD34+fibrocytes, a-smooth muscle antigen-positive myofibroblasts, and CD117 expression in the stroma of invasive squamous cell carcinomas of the oral cavity, pharynx, and larynx, Virchows Arch. 444 (3) (2004) 231–234, http://dx.doi.org/10.1007/s00428–003–0965–1.

[7] I.O. Bello, M. Vered, D. Dayan, A. Dobriyan, R. Yahalom, K. Alanen, P. Nieminen, S. Kantola, E. Läärä, T. Salo, Cancer-associated fibroblasts, a parameter of the tumor microenvironment, overcomes carcinoma-associated parameters in the prognosis of patients with mobile tongue cancer, Oral. Oncol. 47 (1) (2011) 33–38, http://dx.doi.org/10.1016/j.oraloncology.2010.10.013.

[8] C.C. Bitu, J.H. Kauppila, A. Bufalino, S. Nurmenniemi, S. Teppo, M. Keinänen, S.-T. Vilen, P. Lehenkari, P. Nyberg, R.D. Coletta, T. Salo, Cathepsin K is present in invasive oral tongue squamous cell carcinoma *in vivo* and *in vitro*, PLoS One 8 (8) (2013) e70925, http://dx.doi.org/10.1371/journal.pone.0070925.

[9] R. Bussani, F. De-Giorgio, A. Abbate, F. Silvestri, Cardiac metastases, J. Clin. Pathol. 60 (1) (2007) 27–34, http://dx.doi.org/10.1136/jcp.2005.035105.

[10] D.E. Costea, A.O.E. Dimba, L.L. Loro, O.K. Vintermyr, A.C. Johannessen, The phenotype of *in vitro* reconstituted normal human oral epithelium is essentially determined by culture medium, J. Oral. Pathol. Med. 34 (4) (2005) 247–252, http://dx.doi.org/10.1111/j.1600–0714.2005.00308.x.

[11] D. Dayan, T. Salo, S. Salo, P. Nyberg, S. Nurmenniemi, D.E. Costea, M. Vered, Molecular crosstalk between cancer cells and tumor microenvironment components suggests potential targets for new therapeutic approaches in mobile tongue cancer Cancer, Cancer Med. 1 (2) (2012) 128–140, http://dx.doi.org/10.1002/cam4.24.

[12] C. Gaggioli, S. Hooper, C. Hidalgo-Carcedo, R. Grosse, J.F. Marshall, K. Harrington, E. Sahai, Fibroblast-led collective invasion of carcinoma cells with differing roles for RhoGTPases in leading and following cells, Nat. Cell Biol. 9 (12) (2007) 1392–1400, http://dx.doi.org/10.1038/ncb1658.

[13] D. Hanahan, R.A. Weinberg, The hallmarks of cancer, Cell 100 (1) (2000) 57–70, http://dx.doi.org/10.1016/S0092–8674(00)81683–9.

[14] D. Hanahan, R.A. Weinberg, Hallmarks of cancer: the next generation, Cell 144 (5) (2011) 646–674, http://dx.doi.org/10.1016/j.cell.2011.02.013.

[15] M. Heinonen, A. Hemmes, K. Salmenkivi, K. Abdelmohsen, S.-T. Vilén, M. Laakso, M. Leidenius, T. Salo, S. Hautaniemi, M. Gorospe, P. Heikkilä, C. Haglund, A. Ristimäki, Role of RNA binding protein HuR in ductal carcinoma *in situ* of the breast, J. Pathol. 224 (4) (2011) 529–539, http://dx.doi.org/10.1002/path.2889.

[16] Yin Lam King, P. Dickens, A.C.L. Chan, Tumors of the heart: a 20-year

experience with a review of 12 485 consecutive autopsies, Arch. Pathol. Lab. MEd. 117 (10) (1993) 1027–1031.

[17] E.C. Klatt, D.R. Heitz, Cardiac metastases, Cancer 65 (6) (1990) 1456–1459, http://dx.doi.org/10.1002/1097–0142(19900315)65:6 < 1456:: AID-CNCR2820650634 > 3.0.CO;2–5.

[18] M.P. Lewis, K.A. Lygoe, M.L. Nyström, W.P. Anderson, P.M. Speight, J.F. Marshall, G.J. Thomas, Tumour-derived TGF-ß1 modulates myofibroblast differentiation and promotes HGF/SF-dependent invasion of squamous carcinoma cells, Br. J. Cancer 90 (4) (2004) 822–832, http://dx.doi.org/10.1038/sj.bjc.6601611.

[19] T. Mäkelä, F. Yannopoulos, K. Alestalo, J. Mäkelä, P. Lepola, V. Anttila, S. Lehtonen, K. Kiviluoma, R. Takalo, T. Juvonen, P. Lehenkari, Intra-arterial bone marrow mononuclear cell distribution in experimental global brain ischaemia, Scand. Cardiovasc J. 47 (2) (2013) 114–120, http://dx.doi.org/10.3109/14017431.2012.750377.

[20] J. Massagué, TGFβ in Cancer, Cell 134 (2) (2008) 215–230, http://dx.doi.org/10.1016/j.cell.2008.07.001.

[21] K.A. Moutasim, M.L. Nyström, G.J. Thomas, Cell migration and invasion assays, Methods Mol. Biol. 731 (2011) 333–343, http://dx.doi.org/10.1007/978–1-61779–080–5_27.

[22] S. Nurmenniemi, M.-K. Koivula, P. Nyberg, T. Tervahartiala, T. Sorsa, P. S. Mattila, T. Salo, J. Risteli, Type I and III collagen degradation products in serum predict patient survival in head and neck squamous cell carcinoma, Oral. Oncol. 48 (2) (2012) 136–140, http://dx.doi.org/10.1016/j.oraloncology.2011.09.002.

[23] S. Nurmenniemi, T. Sinikumpu, I. Alahuhta, S. Salo, M. Sutinen, M. Santala, J. Risteli, P. Nyberg, T. Salo, A novel organotypic model mimics the tumor microenvironment, Am. J. Pathol. 175 (3) (2009) 1281–1291, http://dx.doi.org/10.2353/ajpath.2009.081110.

[24] E. Pirilä, O. Väyrynen, E. Sundquist, K. Päkkilä, P. Nyberg, S. Nurmenniemi, V. Pääkkönen, P. Pesonen, D. Dayan, M. Vered, L. Uhlin-Hansen, T. Salo, Macrophages modulate migration and invasion of human tongue squamous cell carcinoma, PLoS One 10 (3) (2015) e0120895, http://dx.doi.org/10.1371/journal.pone.0120895.

[25] B. Qiao, N.W. Johnson, J. Gao, Epithelial-mesenchymal transition in oral squamous cell carcinoma triggered by transforming growth factor-ß1 is Snail family-dependent and correlates with matrix metalloproteinase-2 and − 9 expressions, Int. J. Oncol. 37 (3) (2010) 663–668, http://dx.doi.org/10.3892/ijo_00000715.

[26] D.F. Quail, J.A. Joyce, Microenvironmental regulation of tumor progression and metastasis, Nat. Med. 19 (11) (2013) 1423–1437, http://dx.doi.org/10.1038/nm.3394.

[27] N. Rath, M.F. Olson, Rho-associated kinases in tumorigenesis: re-considering ROCK inhibition for cancer therapy, EMBO Rep. 13 (10) (2012) 900–908, http://dx.doi.org/10.1038/embor.2012.127.

[28] K. Reynen, U. Köckeritz, R.H. Strasser, Metastases to the heart, Ann. Oncol. 15 (3) (2004) 375–381, http://dx.doi.org/10.1093/annonc/mdh086.

[29] L. Risteli, J. Risteli, Analysis of extracellular matrix proteins in biological fluids, Methods Enzymol. 145 (1987) 391–411.

[30] S. Salo, C. Bitu, K. Merkku, P. Nyberg, I.O. Bello, J. Vuoristo, M. Sutinen, H. Vähänikkilä, D.E. Costea, J. Kauppila, P. Lehenkari, D. Dayan, M. Vered, J. Risteli, T. Salo, Human bone marrow mesenchymal stem cells induce collagen production and tongue, Cancer Invasion PLoS One 8 (10) (2013) e77692, http://dx.doi.org/10.1371/journal.pone.0077692.

[31] S. Teppo, E. Sundquist, M. Vered, H. Holappa, J. Parkkisenniemi, T. Rinaldi, P. Lehenkari, R. Grenman, D. Dayan, J. Risteli, T. Salo, P. Nyberg, The hypoxic tumor microenvironment regulates invasion of aggressive oral carcinoma cells, Exp. Cell Res. 319 (4) (2013) 376–389, http://dx.doi.org/10.1016/j.yexcr.2012.12.010.

[32] P.A. Torzilli, J.W. Bourne, T. Cigler, C.T. Vincent, A new paradigm for mechan-obiological mechanisms in tumor metastasis, Semin Cancer Biol. 22 (5–6) (2012) 385–395, http://dx.doi.org/10.1016/j.semcancer.2012.05.002.

[33] M. Vered, M. Lehtonen, L. Hotakainen, E. Pirilä, S. Teppo, P. Nyberg, R. Sormunen, A. Zlotogorski-Hurvitz, T. Salo, D. Dayan, Caveolin-1 accumulation in the tongue cancer tumor microenvironment is significantly associated with poor prognosis: an in-vivo and in-vitro study, BMC Cancer 15 (1) (2015) 25, http://dx.doi.org/10.1186/s12885–015–1030–6.